Crystallization Pathways of Sulfate−Nitrate−Ammonium Aerosol Particles

Julie C. Schlenker and Scot T. Martin*

Division of Engineering and Applied Sciences, Harvard University, Cambridge, Massachusetts 02138

Received: June 3, 2005; In Final Form: August 28, 2005

Crystallization experiments are conducted for aerosol particles composed of aqueous mixtures of $(NH_4)_2SO_4$(aq) and NH_4NO_3(aq), $(NH_4)_2SO_4$(aq) and NH_4HSO_4(aq), and NH_4NO_3(aq) and NH_4HSO_4(aq). Depending on the aqueous composition, crystals of $(NH_4)_2SO_4$(s), $(NH_4)_3H(SO_4)_2$(s), NH_4HSO_4(s), NH_4NO_3(s), $2NH_4NO_3{\cdot}(NH_4)_2SO_4$(s), and $3NH_4NO_3{\cdot}(NH_4)_2SO_4$(s) are formed. Although particles of NH_4NO_3(aq) and NH_4HSO_4(aq) do not crystallize even at 1% relative humidity, additions of 0.05 mol fraction SO_4^{2-}(aq) or NO_3^-(aq) ions promote crystallization, respectively. $2NH_4NO_3{\cdot}(NH_4)_2SO_4$(s) and $(NH_4)_3H(SO_4)_2$(s) appear to serve as good heterogeneous nuclei for NH_4NO_3(s) and NH_4HSO_4(s), respectively. $2NH_4NO_3{\cdot}(NH_4)_2SO_4$(s) crystallizes over a greater range of aqueous compositions than $3NH_4NO_3{\cdot}(NH_4)_2SO_4$(s). An infrared aerosol spectrum is provided for each solid based upon a linear decomposition analysis of the recorded spectra. Small nonzero residuals occur in the analysis because aerosol spectra depend on particle morphology, which changes slightly across the range of compositions studied. In addition, several of the mixed compositions crystallize with residual aqueous water of up to 5% particle mass. We attribute this water content to enclosed water pockets. The results provide further insights into the nonlinear crystallization pathways of sulfate−nitrate−ammonium aerosol particles.

1. Introduction

Atmospheric aerosol particles scatter incoming solar radiation directly back to space and serve as cloud condensation nuclei.[1] Sulfate particles are the largest anthropogenic contribution to the global accumulation mode aerosol mass budget and significantly impact Earth's radiation budget in a cooling effect.[2] The physicochemical behavior of the sulfate particles is strongly influenced by the presence of nitrate and ammonium.[3] In particular, the aqueous versus crystalline phase of particles depends strongly on chemical composition. Phase, in turn, significantly impacts radiative forcing and atmospheric chemistry. For instance, given initial dry particle size distributions of 50 to 200 nm in diameter, which are typical in the troposphere, aqueous particles scatter solar radiation more efficiently than do crystalline particles.[4] Sulfate particles also affect atmospheric chemistry by serving as a medium for heterogeneous reactions, such as N_2O_5 hydrolysis,[5] which occur faster on aqueous particles than on crystalline particles.[6−8] Knowledge of particle physical state is thus required to accurately determine the effects of sulfate, nitrate, ammonium, and proton (SNA) particles on radiative forcing and atmospheric chemistry.[9,10]

We have published two previous reports on laboratory studies of the phase changes of SNA particles. In our first report, we measured the crystallization relative humidities (CRH) of SNA particles.[11] The black-and-white squares and circles in Figure 1 show compositions that did and did not crystallize, respectively. In a second report, we identified which solids formed for compositions that did crystallize.[12] The six solids included $(NH_4)_2SO_4$ (AS), $(NH_4)_3H(SO_4)_2$ (LET), NH_4HSO_4 (AHS), NH_4NO_3 (AN), $2NH_4NO_3{\cdot}(NH_4)_2SO_4$ (2AN·AS), and $3NH_4NO_3{\cdot}(NH_4)_2SO_4$ (3AN·AS). Using a linear algebra approach to deconvolute the spectra recorded in the presence of two or three solids, we determined the infrared peak positions and strengths for each of these solids and reported the results in a table.

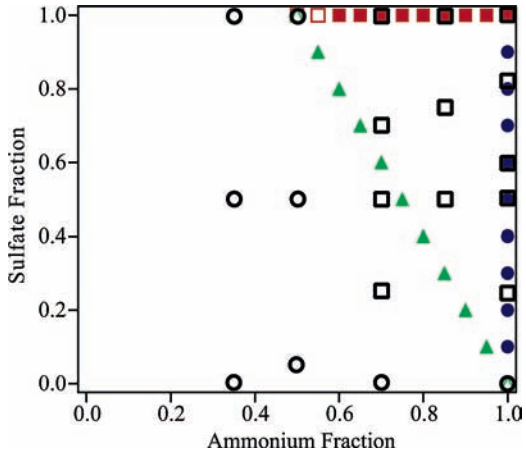

Figure 1. Summary of compositions studied. Legend: closed colored symbols (●, ■, ▲) show compositions that crystallized in this study; open colored symbols (○, □, △) show compositions that did not crystallize in this study even at 3% RH; black-and-white circles (○) show compositions that did not crystallize even at 1% RH in the study of Martin et al.[11]; and black-and-white squares (□) show compositions that crystallized in the studies of Schlenker et al.[12] and Martin et al.[11] The study of Schlenker et al.[12] also identified the crystals formed at compositions specified by the symbols □.

For the current study, by carrying out new measurements of particular composition regions in the SNA system, we derive aerosol infrared spectra of the six solids. Reference aerosol spectra are not available for some of the solids because they do not crystallize homogeneously. Therefore, derivation of the spectra through linear deconvolution of the recorded spectra is necessary. In our previous work, we were unable to resolve some

* To whom correspondence should be addressed. E-mail: scot_martin@harvard.edu. http://www.deas.harvard.edu/environmental-chemistry.

10.1021/jp052973x CCC: $30.25
Published on Web 10/14/2005

of the overlapping peaks because of wide spacing among the investigated chemical compositions (Figure 1, black-and-white points). In the current study, finer spacing (Figure 1, color points) allows us to resolve these overlapping peaks and thus derive complete spectra. The finer spacing also allows for the development of more detailed constraints on the crystallization pathways of the SNA particles.

2. Experimental Approach

2.1. Chemical Compositions Studied. The 30 filled symbols in Figure 1 show the SNA chemical compositions studied. The chemical composition is described by $X-Y$ coordinates.[9,10,13] X is the fraction of cations due to ammonium with the balance coming from proton (i.e., the degree of neutralization). Y is the fraction of anions due to sulfate with the balance coming from nitrate. Namely,

$$X = \text{moles of } NH_4^+/(\text{moles of } NH_4^+ + \text{moles of } H^+) \quad (1a)$$

$$Y = \text{moles of } SO_4^{2-}/(\text{moles of } SO_4^{2-} + \text{moles of } NO_3^-) \quad (1b)$$

Therefore, the axis of $X = 1$ describes particles having neutral compositions and varying amounts of sulfate and nitrate. The axis of $Y = 1$ describes particles having varying amounts of $(NH_4)_2SO_4$ and H_2SO_4 and no nitrate. Throughout this paper, aerosol particle chemical composition is denoted as [X, Y]. $(NH_4)_2SO_4$, for example, has the composition [1, 1], and $(NH_4)NO_3$ has the composition [1, 0].

2.2. Collection of Aerosol Spectra. The experimental apparatus has been described previously.[12] Aqueous aerosol particles of composition [X, Y] were produced with a TSI 3076 atomizer from 1 M reservoir solutions of composition [X, Y]. The aerosol flowed in atmospheric pressure at 3 L min^{-1} through a series of RH-controlled cells, which served to program an aerosol RH history. Specifically, except when noted otherwise, the aerosol particles in the current study were exposed at 293 K to an RH history of 60% for 210 s, followed by 3% for 210 s, followed by 30% for 270 s, which is denoted hereafter in shorthand as 60 → 3 → 30%. The strategy of this experimental protocol was to take advantage of the hysteresis effect to unambiguously determine if crystallization had occurred. Namely, particles that fully crystallized at 3% RH did not take up liquid water in the final RH cell at 30% provided that the deliquescence relative humidity (DRH) was not exceeded. According to the Aerosol Inorganics Model (AIM), AHS had the lowest initial DRH of the SNA solids, which was a peritonic transition to LET at 38% RH at 293 K.[3] Other peritonic and eutonic values were also greater than 30% RH (cf. Figure 8).

Particle phase and the crystals formed were determined by analysis of infrared extinction spectra. The extinction spectra were recorded (software in absorbance mode, 1000 scans, 1 cm^{-1} resolution) when the RH-processed aerosol flowed into a 90-cm detection cell. Extinction resulted both from the absorbance by gases and particles and from the scattering by particles. Reference gas-phase water absorbance spectra were subtracted from the extinction spectra, leaving residual spectra of the condensed-phase aerosol constituents. The reference gas-phase water spectra, obtained by exposing a particle-free N_2-flow to the same RH program as the aerosol, were collected before and after each aerosol experiment. Spectra shown in the figures of this paper are those of the condensed-phase aerosol constituents.

3. Results and Discussion

3.1. Crystallization. Spectral results, for aerosol particles having compositions ranging from $(NH_4)_2SO_4$ to NH_4NO_3 by replacement of SO_4^{2-} with NO_3^- in steps of $\Delta Y = 0.1$ along the [1.0, Y] axis, are shown in Figure 2. The particles are exposed to an RH program of 60 → 3 → 30%. Only the spectrum collected for NH_4NO_3 (i.e., [1.0, 0.0]) shows liquid water at 30% RH. The absence of liquid water in the remaining spectra indicates that the aerosol particles of [1.0, Y] crystallize for $Y \geq 0.1$.

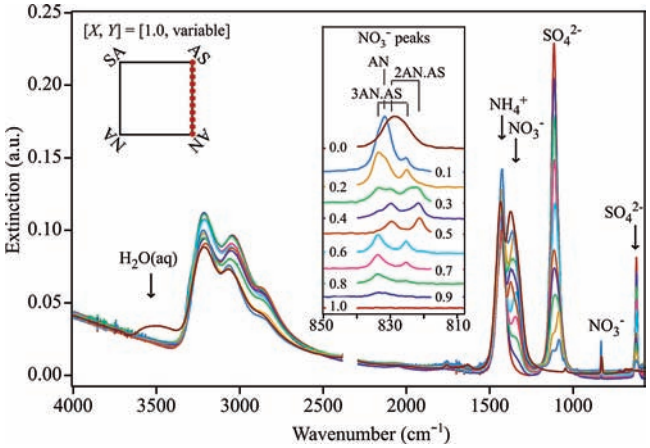

Figure 2. Spectral results for aerosol particles composed of mixtures of NH_4NO_3 and $(NH_4)_2SO_4$ after exposure to an RH history of 60 → 3 → 30%. The [X, Y] composition is varied in these experiments from [1.0, 0.0] to [1.0, 1.0] in steps of [+0.00, +0.10]. The inset shows the NO_3^- peaks for AN, 2AN·AS, 3AN·AS, and aqueous NH_4NO_3.

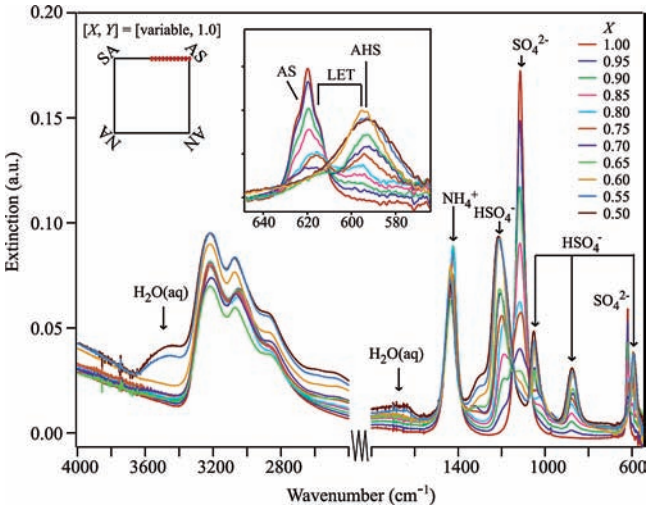

Figure 3. Spectral results for aerosol particles composed of mixtures of NH_4HSO_4 and $(NH_4)_2SO_4$ after exposure to an RH history of 60 → 3 → 30%. The [X, Y] composition is varied in these experiments from [0.5, 1.0] to [1.0, 1.0] in steps of [+0.05, +0.00]. The inset shows the SO_4^{2-} and HSO_4^- peaks.

Interpretation of the spectral results indicates which crystals form at 30% RH. For example, peak positions in the 820 to 835 cm^{-1} spectral window are unique signatures of 2AN·AS, 3AN·AS, and AN.[12] From $Y = 0.9$ to 0.6, NO_3^- peaks occur at 825 and 834 cm^{-1}, indicative of 2AN·AS. At $Y = 0.5$, the peaks at 821 and 830 cm^{-1} arise from 3AN·AS. At $Y = 0.2$, the intense peak at 831 cm^{-1} implicates the presence of AN. The broad NO_3^- peak at $Y = 0$ arises from aqueous nitrate. Shifts in the NO_3^- peaks in the 1350 to 1380 cm^{-1} spectral window also occur as the predominant NO_3^- solid changes.

Figure 3 shows the spectral results for a set of experiments in which the particle composition varies from pure $(NH_4)_2SO_4$ to pure NH_4HSO_4 in steps of $\Delta X = -0.05$ from [1.0, 1.0] to [0.5, 1.0]. Liquid water is observed in several spectra. Particles

with compositions of $X = 0.50$ and 0.55 are completely aqueous after processing by an RH program of 60 → 3 → 30%. Namely, the spectra of this RH program for $X = 0.50$ and 0.55 are identical with those of a program of 60 → 30% (data not shown but see Figure 3 of ref 12 for an example at $X = 0.50$). Furthermore, a small amount of liquid water is also observed for particles having compositions of $X = 0.60$, 0.65, and 0.70. Integration of the OH stretch at 3500 cm^{-1} shows that the liquid water is less than 5% of the fully aqueous aerosol. Therefore, at least some of the aerosol consists of mixed crystalline and aqueous particles. For $X > 0.70$, no liquid water is observed. Thus, depending on the composition, the aerosol particles at 30% RH are completely aqueous, dominantly crystalline but with some aqueous content, or completely solid.

The 580 to 630 cm^{-1} spectral window of Figure 3 shows SO_4^{2-} and HSO_4^- peaks indicative of AS, LET, and AHS. For example, from $X = 1.0$ to 0.8, a sharp SO_4^{2-} peak occurs at 619 cm^{-1}, indicating that AS is present. The strength of this peak decreases as X decreases. From $X = 0.95$ to 0.75, the growth of the peak at 596 cm^{-1} and of shoulders around 619 cm^{-1} shows increasing amounts of LET. At $X = 0.70$, the shift of the peak from 596 to 593 cm^{-1} and the appearance of a shoulder at 589 cm^{-1} indicate that AHS forms. The broad peak at 592 cm^{-1} for $X = 0.55$ and 0.50 is due to aqueous HSO_4^-.

The aerosol of dominant crystalline but some aqueous content for $X = 0.60$, 0.65, and 0.70 can arise from either internal or external mixing. Internal mixing describes an aerosol containing individually similar particles whereas external mixing describes an aerosol having two or more dissimilar particle types.[1] In the present case, the low water content indicates that greater than 95% of aerosol particle mass is AHS and LET. The remaining 5% (upper limit) of water mass, if internally mixed with the solids, would require that the aqueous phase, which would be metastable toward crystallization, be in contact with one or both of LET and AHS.

The aqueous phase of an internally mixed particle could occur as an outer aqueous layer or instead as enclosed pockets of liquid in an otherwise crystalline particle.[14] Specifically, internally mixed particles of three types can be considered: an acid-enriched outer aqueous layer on LET, an alkaline-enriched outer aqueous layer on AHS, or an AHS/LET particle having pockets of liquid aqueous phase. The first two particle types appear ruled out because heterogeneous nucleation by LET or AHS could be expected to initiate crystallization of an outer aqueous layer. Moreover, we further rule out the second particle type because LET should form prior to AHS. In contrast, the third particle type appears to be a very reasonable suggestion because efflorescence of the aqueous-phase pockets would be inhibited since water would not evaporate. The formation of liquid pockets would be increasingly favorable in the larger particles of the aerosol size distribution.[15,16]

The alternative is that the 5% water content arises from external mixing, having in the aerosol a less numerous population of aqueous particles of composition $X = 0.60$ and a more numerous population of internally mixed solid particles of 40% LET and 60% AHS. Under this description, however, the fraction of aqueous particles should depend on residence time because homogeneous nucleation should lead to their crystallization. We do not observe a dependence on residence time. Given the weight of the factors, we believe that the physically most reasonable model is that the 5% water mass arises from aqueous pockets trapped inside the larger particles of the aerosol size distribution.

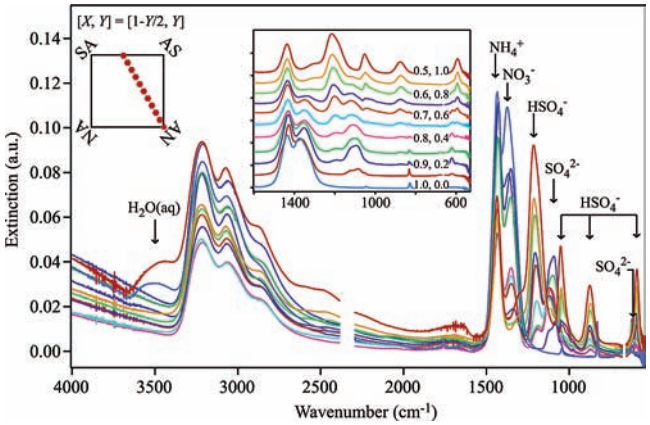

Figure 4. Spectral results for aerosol particles composed of mixtures of NH_4HSO_4 and NH_4NO_3 after exposure to an RH history of 60 → 3 → 30%. The [*X*, *Y*] composition is varied in these experiments from [0.5, 1.0] to [1.0, 0.0] in steps of [+0.05, −0.10]. The inset shows the changes in peaks from 550 to 1600 cm^{-1}.

Figure 4 shows the spectra recorded at 30% RH for chemical compositions along the transect from pure NH_4HSO_4 to pure NH_4NO_3 in 10 steps of [+0.05, −0.10] from [0.5, 1.0] to [1.0, 0.0]. Pure aqueous NH_4HSO_4 and pure aqueous NH_4NO_3 do not crystallize, as shown by the large liquid water content at 30% RH. For these two compositions, the water content for a history of 60 → 3 → 30% is the same as that of 60 → 30% (data not shown here but see Figure 3 of ref 12). Other chemical compositions along the transect, however, crystallize completely, with the exception of [0.55, 0.90] and [0.95, 0.1] that have a mixed crystalline/aqueous aerosol of less than 5% water mass. By the same line of reasoning as given above, aqueous pockets trapped inside the larger particles are the apparent explanation.

3.2. Derived Infrared Spectra. A subset of the data shown in Figures 2 to 4 is employed to derive infrared spectra of the contributing solid phases (Figure 5). The subset includes the spectra having no liquid water (i.e., 20 out of 30 spectra). The analysis assumes that each recorded spectrum is a linear combination of basis spectra (i.e., one for each solid) and that each basis spectrum consists of multiple Lorentzian peaks (i.e., the characteristic infrared spectrum). Lorentzian peaks are described by

$$E_{ij}(\tilde{\nu}) = \frac{A_{ij}}{1 + 4\left(\frac{\tilde{\nu} - (\tilde{\nu}_0)_{ij}}{\Gamma_{ij}}\right)^2} \qquad (2)$$

where E is extinction, $\tilde{\nu}$ is wavenumber, A is band amplitude, $\tilde{\nu}_0$ is band center, and Γ is band full width at half-maximum.[17] A solid is denoted by i and a characteristic peak by j.

The spectra shown in Figures 2−4 are decomposed by this analysis as

$$E_k(\tilde{\nu}) = \sum_{i=1}^{N}(\alpha_{ik}\sum_{j=1}^{n_i}E_{ij}(\tilde{\nu})) \qquad (3)$$

where k is the label of a specific recorded spectrum, N is the total number of spectra in the basis set, n_i is the total number of peaks in basis spectrum i, and α_{ik} is the loading of solid i in spectrum k.

As a practical matter, eq 3 is stepwise fit to Figures 2 through 4. The data in Figure 2 are first analyzed. The values for N and n_i are chosen by human observation of the spectra, and the data in Figure 2 for 550 < $\tilde{\nu}$ < 1650 cm^{-1} and all k are then fit

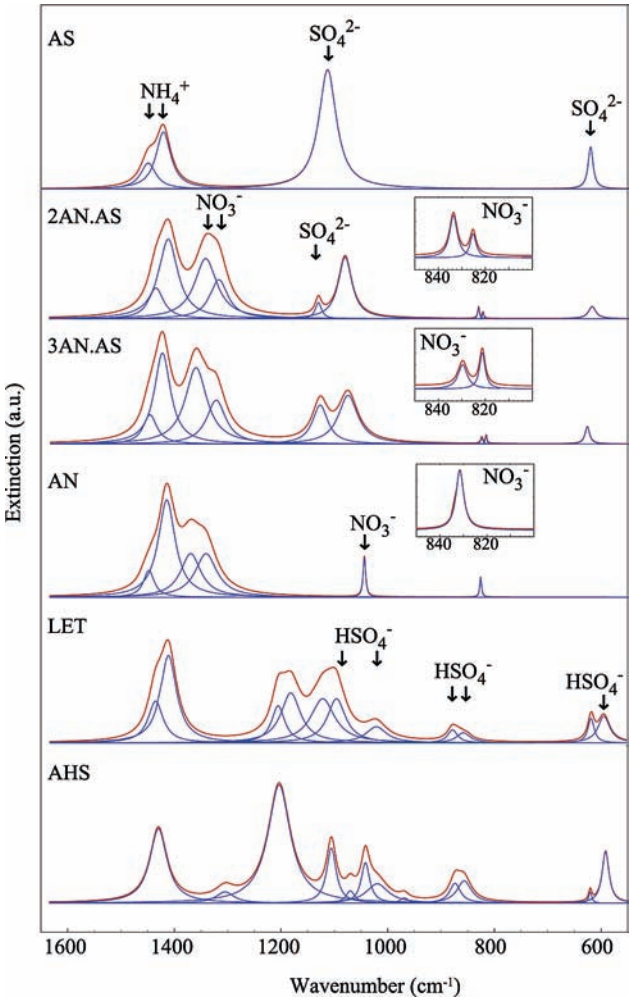

Figure 5. Derived infrared spectra of AS, 2AN·AS, 3AN·AS, AN, LET, and AHS. The red lines show the derived spectra (eq 3). The blue lines show the individual peaks (eq 2).

globally by eqs 2 and 3 for A_{ij}, Γ_{ij}, $(\tilde{\nu}_0)_{ij}$, and α_{ik} in a *Mathematica*-based algorithm. Four solids are known over the range of chemical compositions shown in Figure 2, and the data require that $N = 4$ for small residuals. The resulting derived aerosol infrared spectra i are assigned to AS, 2AN·AS, 3AN·AS, and AN based upon the k-value (which is a surrogate for chemical composition Y in Figure 2) at which α_{ik} is maximum. The derived and assigned spectra are shown in Figure 5. Similar analysis for Figure 3 requires $N = 3$, and the resulting spectra of AS, LET, and AHS are shown in Figure 5. Finally, analysis of Figure 4 requires that $N = 4$, and the derived spectra agree with those derived for AHS, LET, 2AN·AS, and AN from Figures 2 and 3.

The derived spectra can be compared to several reports in the literature. The aerosol spectra reported in the literature[18,19] for AS in the low scattering regime (i.e., particles smaller than approximately 1 μm) are in excellent agreement with AS shown in Figure 5. We know of no other reports of aerosol spectra for the other solids. The AN,[20−23] LET,[24,25] and AHS[20,26] spectra are, however, broadly consistent with transmission measurements of thin films and particles suspended in Nujol as well as diffuse reflectance measurements of powders. Apparent differences among spectra collected in these various geometries (including the aerosol measurements) can generally be rationalized by the relative contributions of the real and imaginary parts of the refractive index to the measurement.[27−31] We know of

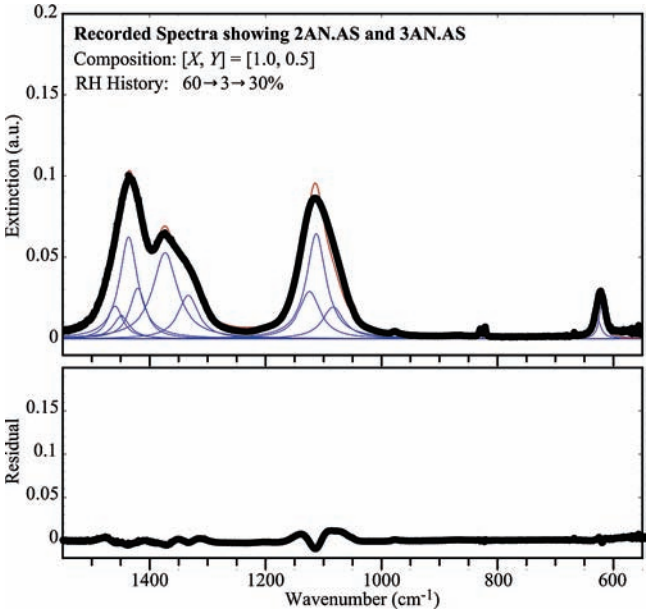

Figure 6. Spectral fit and small but nonzero residual for composition [1.0, 0.5].

no literature reports of the infrared spectra of 2AN·AS and 3AN·AS, except for the table of peak positions we previously published.[12]

The residuals following application of eq 3 to the recorded spectra are small but nonzero (e.g., Figure 6 and other examples in the Supporting Information). The residuals are too small and inconsistent to suggest an undiscovered solid, yet they are too significant to accept that they are random noise. The explanation is that differing particle morphologies affect extinction. The same chemical solid of fixed inherent optical constants may crystallize differently (e.g., internal versus external mixing, shell-core versus microcrystalline, or oblate/prolate versus spherical) from an aqueous solution of composition $[X_1, Y_1]$ compared to one of composition $[X_2, Y_2]$. Fixed basis spectra, therefore, do not underlie crystallization from all $X-Y$ compositions, and small residuals in a linear analysis are expected from this nonlinearity.

A quantitative example of some of these effects on a residual is shown in Figure 7. Particle diameter, optical constants of A and B, and mass of A and B are held constant in the calculations. The optical constants of B are those of A but offset by 100 cm^{-1}. The spectra are simulated by using Mie scattering equations.[27] Type I aerosol, which is an external mixture of the solids, is simulated by calculating the spectra of A and B and taking the sum. Type II aerosol, which consists of internally mixed microcrystalline particles, is simulated by calculating the spectrum after averaging the optical constants of A and B. Type III aerosol, which consists of internally mixed particles of core−shell morphology, is simulated by assuming A is the core and B is the shell. Difference spectra between the simulations of type II and type I and of type III and type I are shown in the bottom of Figure 7. The nonzero differences indicate that the morphologies of the particles affect the aerosol extinction spectrum. The assumption of a linear basis set is, therefore, an approximation of limited accuracy if particle morphology changes.

An example of the effects of oblate versus prolate particles on aerosol extinction is provided by Wagner et al.[31] Figure 8 therein shows the effects of shape on peak amplitude, position, and width for the same set of underlying optical constants for a particle having a volume-equivalent diameter of 100 nm. In

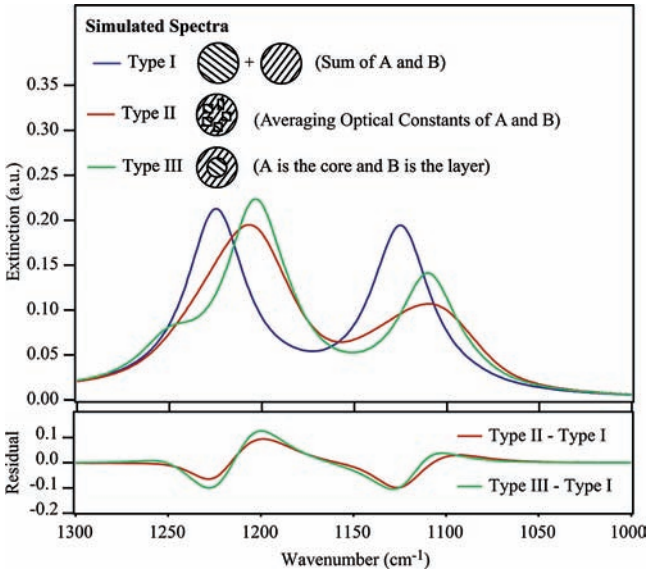

Figure 7. Simulated spectra and their differences for aerosol particles composed of species A and B in particle morphologies I to III, as depicted in the figure: type I, external mixture; type II, microcrystalline internal mixture; and type III, core−shell internal mixture.

particular, Wagner et al. show that the ratio of two nearby peaks changes significantly with the aspect ratio of the particle. When particle shape and therefore relative band amplitude change with crystallization from different $X-Y$ compositions, analysis with a linear basis is not completely accurate and leads to small nonzero residuals.

3.3. Conclusions. The deliquescence and crystallization properties of SNA particles are summarized in Figure 8. These results further refine our earlier report[12] that AN and AHS can form in aqueous aerosol particles when another solid forms first and subsequently serves as a good heterogeneous nucleus, namely 2AN·AS for AN and LET for AHS. In the earlier report, the coarse grid spacing of the compositions studied allowed us to say that, although AN certainly formed at [0.70, 0.50], it possibly formed at [1.0, 0.25]. The finer grid spacing of this study coupled with the improved spectral analysis allows us to definitively conclude that AN forms for $Y \geq 0.10$ for compositions of [1.0, Y] and that the threshold point for AN formation lies between $0 < Y < 0.10$. Similarly, the earlier work coarsely established that AHS can form in compositions of [0.70, 1.0], and the present work refines the onset composition to $0.55 < X < 0.60$ along the axis of [X, 1.0].

The pie charts in Figure 8 show that 2AN·AS nucleates more readily than 3AN·AS for many compositions, even at several nitrate-enriched compositions for which the supersaturation of 3AN·AS is likely greater than that of 2AN·AS. As a result, 2AN·AS is present in 8 of 11 compositions studied between pure NH_4NO_3 and pure $(NH_4)_2SO_4$, which could suggest its formation is also frequent in atmospheric particles. Similarly, 2AN·AS is the dominant solid, compared to 3AN·AS, along the transect from AN to AHS. For several compositions, the spectra show signatures of more solids than are allowed by the Gibbs phase rule. In these cases, we infer external mixtures of two different particle types.[12] External mixing is indicated in Figure 8 by having two pie charts.

A final observation is that, contrary to conventional wisdom, impurities of order 5% tend to induce rather than inhibit crystallization, even though supersaturation is reduced. For example, whereas [0.55, 1.0] remains aqueous for an RH program of 60 → 3 → 30%, [0.55, 0.90] forms crystalline

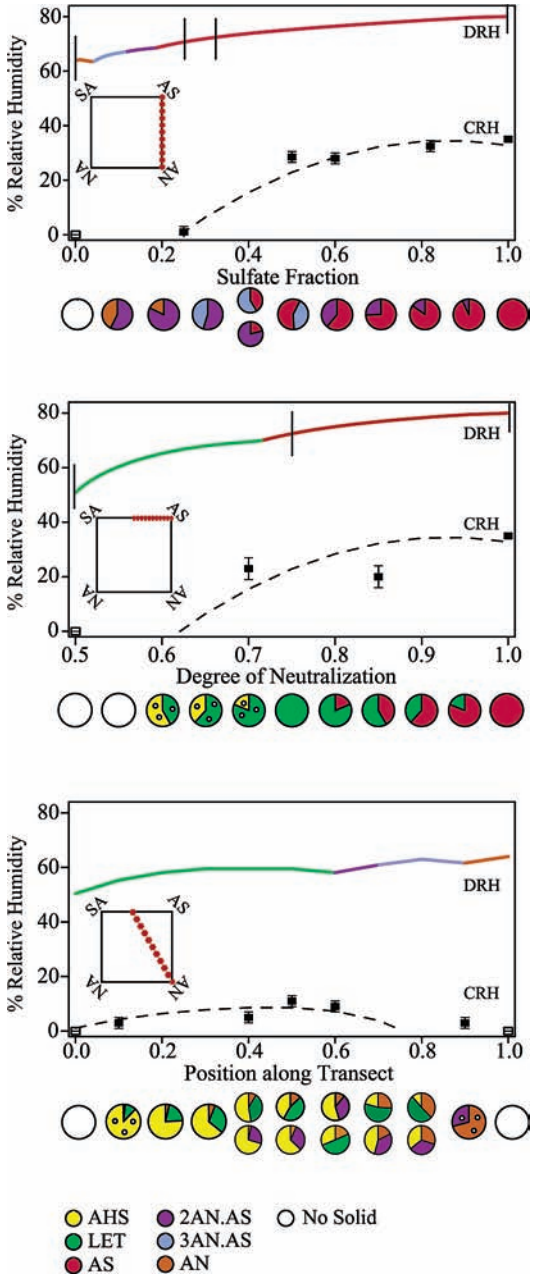

Figure 8. Summary of results along three $X-Y$ transects (cf. Figure 1). Solid lines show complete deliquescence according to the predictions of the Aerosol Inorganics Model.[3] The color of the line indicates the final solid to dissolve. The black vertical lines indicate stoichiometric positions of solids, corresponding to AN, 3AN·AS, 2AN·AS, and AS in the top panel and AHS, LET, and AS in the middle panel. The dashed black lines show the crystalllization relative humidity obtained from the CRH polynomial of Martin et al.[11] The black squares show the CRH data points of Martin et al.[11] The pie charts below each panel show the relative mass of each solid in the crystallized particles based upon the identification of the solids from the infrared spectra recorded at 30% relative humidity and the partitioning of the solids according to mass balance. Open pie charts show compositions that do not crystallize even at 1% relative humidity. Pies having small white circles indicate compositions that crystallize by at least 95% of the particle mass and are inferred to have trapped, nonefflorescd aqueous pockets of less than 5% of the particle mass.

particles when subjected to a similar RH program. Therefore, NO_3^- ion helps to induce crystallization. Alternatively, at the other end of the transect, [1.0, 0.0] does not crystallize but the addition of SO_4^{2-} for [1.0, 0.10] leads to crystallization as does the addition of H^+ and SO_4^{2-} at [0.95, 0.10]. How dissolved

components such as NO_3^-, H^+, or SO_4^{2-} promote crystallization is an outstanding challenge for theoretical study in this field of research, although the hypothesis is that these nonlinear effects lie in ternary or higher germ formation and/or changes in the surface tensions of incipient crystals by adsorption. Other dissolved constituents in atmospheric particles may also be supposed to induce crystallization.

Acknowledgment. We are grateful for support received from the NSF Atmospheric Chemistry Program (ATM-0317583).

Supporting Information Available: The recorded infrared spectra (Figures 2−4) and the derived infrared spectra of SNA solids (Figure 5). This material is available free of charge via the Internet at http://pubs.acs.org.

References and Notes

(1) Seinfeld, J. H.; Pandis, S. N. *Atmospheric Chemistry and Physics*: *From Air Pollution to Climate Change*; Wiley: New York, 1998.

(2) Penner, J. E.; Andreae, M.; Annegarn, H.; Barrie, L.; Feichter, J.; Hegg, D.; Jayaraman, A.; Leaitch, R.; Murphy, D.; Nganga, J.; Pitari, G. Aerosols, their Direct and Indirect Effects. In *In Climate Change 2001*: *The Scientific Basis. Contribution of Working Group I to the Third Assessment Report of the Intergovernmental Panel on Climate Change*; Houghton, J. T., Ding, Y., Griggs, D. J., Noguer, M., Linden, P. J., Dai, X., Maskell, K., Johnson, C. A., Eds.; Cambridge University Press: New York, 2001; pp 289−348.

(3) Clegg, S. L.; Brimblecombe, P.; Wexler, A. S. *J. Phys. Chem. A* **1998**, *102*, 2137−2154.

(4) Hegg, D.; Larson, T.; Yuen, P. F. *J. Geophys. Res.* **1993**, *98*, 18435−18439.

(5) Mozurkewich, M.; Calvert, J. G. *J. Geophys. Res.* **1988**, *93*, 15889.

(6) Kane, S. M.; Caloz, F.; Leu, M. T. *J. Phys. Chem. A* **2001**, *105*, 6465−6470.

(7) Hallquist, M.; Stewart, D. J.; Stephenson, S. K.; Cox, R. A. *Phys. Chem. Chem. Phys* **2003**, *5*, 3453−3463.

(8) Thornton, J. A.; Braban, C. F.; Abbatt, J. P. D. *Phys. Chem. Chem. Phys* **2003**, *5*, 4593−4603.

(9) Martin, S. T. *Chem. Rev.* **2000**, *100*, 3403−3453.

(10) Martin, S. T.; Hung, H. M.; Park, R. J.; Jacob, D. J.; Spurr, R. J. D.; Chance, K. V.; Chin, M. *Atmos. Chem. Phys.* **2004**, *4*, 183-214.

(11) Martin, S. T.; Schlenker, J. C.; Malinowski, A.; Hung, H. M.; Rudich, Y. *Geophys. Res. Lett.* **2003**, *30*, 2102.

(12) Schlenker, J. C.; Malinowski, A.; Hung H. M.; Rudich, Y. *J. Phys. Chem. A* **2004**, *108*, 9375−9383.

(13) Potukuchi, S.; Wexler, A. S. *Atmos. Environ.* **1995**, *29*, 3357−3364.

(14) Weis, D. D.; Ewing, G. E. *J. Geophys. Res.* **1999**, *104*, 21275−21285.

(15) Charlesworth, D. H.; Marshall, W. R. *AIChE J.* **1960**, *6*, 9−23.

(16) Colberg, C. A.; Krieger, U. K.; Peter, T. *J. Phys. Chem. A* **2004**, *108*, 2700−2709.

(17) Weis, D. D.; Ewing, G. E. *J. Geophys. Res.* **1996**, *101*, 18709−18720.

(18) Cziczo, D. J.; Abbatt, J. P. D. *J. Geophys. Res.* **1999**, *104*, 13781−13790.

(19) Onasch, T. B.; Siefert, R. L.; Brooks, S. D.; Prenni, A. J.; Murray, B.; Wilson, M. A.; Tolbert, M. A. *J. Geophys. Res.* **1999**, *104*, 21317−21326.

(20) Miller, F. A.; Wilkins, C. H. *Anal. Chem.* **1952**, *24*, 1253−1294.

(21) Kearley, G. J.; Kettle, S. F. A. *J. Chem. Phys.* **1980**, *73*, 2129−2136.

(22) Jarzembski, M. A.; Norman, M. L.; Fuller, K. A.; Srivastava, V.; Cutten, D. R. *Appl. Opt.* **2003**, *42*, 922−930.

(23) Shilling, J. E.; Tolbert, M. A. *J. Phys. Chem. A* **2004**, *108*, 11314−11320.

(24) Damak, M.; Kamoun, M.; Daoud, A.; Romain, F.; Lautie, A.; Novak, A. *J. Mol. Struct.* **1985**, *130*, 245−254.

(25) Kamoun, M.; Lautie, A.; Romain, F.; Novak, A. *J. Raman Spectrosc.* **1988**, *19*, 329−335.

(26) Cziczo, D. J.; Abbatt, J. P. D. *J. Phys. Chem. A* **2000**, *104*, 2038−2047.

(27) Bohren, C. F.; Huffman, D. R. *Absorption and Scattering of Light by Small Particles*; Wiley: New York, 1983.

(28) Griffiths, P. R.; De Haseth, J. A. *Fourier Transform Infrared Spectrometry*; Wiley: New York, 1986.

(29) Colthup, N. B.; Daly, L. H.; Wiberley, S. E. *Introduction to Infrared and Raman Spectroscopy*; Academic: New York, 1990.

(30) Urban, M. W. *Attenuated Total Reflectance Spectroscopy of Polymers*: *Theory and Practice*; American Chemical Society: Washington, D.C., 1996.

(31) Wagner, R.; Mohler, O.; Saathoff, H.; Stetzer, O.; Schurath, U. *J. Phys. Chem. A* **2005**, *109*, 2572−2581.